Journal of Materials Chemistry A

PAPER

View Article Online
View Journal | View Issue



Cite this: J. Mater. Chem. A, 2014, 2, 20231

# Carbon-coated rhombohedral $Li_3V_2(PO_4)_3$ as both cathode and anode materials for lithium-ion batteries: electrochemical performance and lithium storage mechanism†

Zelang Jian,‡[a] Wenze Han,‡[b] Yanliang Liang,[a] Yucheng Lan,[c] Zheng Fang,[d] Yong-Sheng Hu[d] and Yan Yao*[ae]

Received 9th September 2014
Accepted 5th October 2014

DOI: 10.1039/c4ta04630g

www.rsc.org/MaterialsA

We report the electrochemical performance and storage mechanism of a symmetrical lithium-ion battery made of carbon-coated rhombohedral $Li_3V_2(PO_4)_3$ (r-LVP/C) as both the cathode and anode materials. The electrochemical evaluation of r-LVP/C in lithium half-cells demonstrates reversible lithium extraction/insertion reactions at 3.75 V and average 1.75 V *vs.* $Li^+/Li$. Different storage mechanisms for the two reactions have been identified through *ex situ* and *in situ* X-ray diffraction measurements. A two-phase reaction takes place when two Li are extracted from r-LVP/C, while a solid-solution reaction occurs when two Li are inserted into r-LVP/C. In comparison, only one Na ion can be inserted into its sodium counterpart, $Na_3V_2(PO_4)_3$. Symmetrical batteries presented a high capacity of 120 mA h $g^{-1}$ with an operating voltage of ~2.0 V.

## 1. Introduction

In the last two decades, lithium-ion batteries (LIBs) have attracted significant attention because of their high energy/power density and broad application in consumer electronics and electric vehicles.[1–5] Due to their promising electrochemical power for energy storage and conversion devices, LIBs have been widely used in high-power consumer devices, such as laptops, cameras, mobile phones and electric vehicles.[6–8]

Polyanion-type $LiFePO_4$ has been used in power tools and electric vehicles because of its stable structure and favorable electrochemical properties.[9–11] Other polyanion-type materials, such as $LiMPO_4$ (M = Mn, Co, Ni),[12–14] $Li_3M_2(PO_4)_3$ (M = V, Fe, Ti),[15–19] $Li_9M_3(PO_4)_2(P_2O_7)_3$ (M = V, Cr, Al, Ga)[20,21] and $Li_2MP_2O_7$ (M = Mn, Co, Fe),[22,23] have also been extensively investigated due to their significant thermal stability and competitive energy density. Among these materials, $Li_3M_2(PO_4)_3$ (M = V, Fe, Ti) has attracted considerable attention due to its covalent three-dimensional structure with high ionic conductivity.[24–27] In particular, $Li_3V_2(PO_4)_3$ has been synthesized in two different forms: monoclinic $Li_3V_2(PO_4)_3$ (m-LVP) and rhombohedral $Li_3V_2(PO_4)_3$ (r-LVP).[19,28,29] m-LVP is the stable phase synthesized directly from a high-temperature solid-state reaction. The theoretical capacity is 131 mA h $g^{-1}$, corresponding to the extraction of two $Li^+$ ions. However, m-LVP exhibits multiple plateaus in the discharge curves at 4.1, 3.7, and 3.6 V.[30–32] In comparison, r-LVP shows more appealing discharge curves with a very flat plateau at 3.75 V *vs.* $Li^+/Li$, although it cannot be directly synthesized. Nazar *et al.* first reported the synthesis of r-LVP through a topotactic ion exchange from r-$Na_3V_2(PO_4)_3$ in concentrated $LiNO_3$ solution. 1.3 Li (corresponding to 85 mA h $g^{-1}$) were reported to be reversibly inserted back into the structure after the first 2 Li extraction.[28]

Rhombohedral NASICON structures with a $V^{4+}/V^{3+}$ redox couple have long been identified as candidates for high-voltage cathode,[15,28,36] but there has been no report on using r-LVP as an anode material. In $Li_3V_2(PO_4)_3$, vanadium is in its intermediate valence state III, which can form two redox couples, $V^{4+}/V^{3+}$ and $V^{3+}/V^{2+}$. $Li^+$ ions not only can be extracted from the $Li_3V_2(PO_4)_3$ structure, but also can be further inserted into the structure. It has been reported that two additional Li can be inserted into the NASICON structure in the solid-solution fashion: $LiTi_2(PO_4)_3$[16] at an average potential around 1.6 V *vs.* $Li^+/Li$ or $Li_3Fe_2(PO_4)_3$[17] at an average potential around 2.75 V *vs.* $Li^+/Li$. However, the

[a]Department of Electrical and Computer Engineering, University of Houston, Houston, Texas 77204, USA. E-mail: yyao4@uh.edu

[b]China Institute of Atomic Energy, Beijing 102413, China

[c]Department of Physics and Engineering Physics, Morgan State University, Baltimore, MD 21251, USA

[d]Key Laboratory for Renewable Energy, Beijing Key Laboratory for New Energy Materials and Devices, Beijing National Laboratory for Condensed Matter Physics, Institute of Physics, Chinese Academy of Sciences, Beijing 100190, China

[e]Texas Center for Superconductivity at The University of Houston, Houston, Texas 77204, USA

† Electronic Supplementary Information (ESI) available: Crystallographic data of the r-LVP/C; magnified XRD pattern of r-LVP/C; TG curves of r-NVP/C and r-LVP/C; SEM images of r-NVP/C and r-LVP/C; typical discharge/charge of r-NVP/C as anode. See DOI: 10.1039/c4ta04630g

‡ Z. L. Jian and W. Z. Han contributed equally to this work.

sodium counterpart of r-LVP can only accommodate one additional Na at 1.63 V *vs.* $Na^+/Na$.[37,38] All these observations lead us to investigate the plausibility of exploring r-LVP as an anode material for lithium storage.

In this work, carbon-coated r-LVP (r-LVP/C) was obtained by an ion exchange method from r-NVP/C in a commercial electrolyte for LIBs. The carbon-coating strategy has been applied to various electrode materials to improve the electronic conductivity and protect the active materials.[33–35] We studied the structure of Li atomic site occupation in the r-LVP structure deduced from Rietveld-refined X-ray diffraction results. This material shows a flat plateau at 3.75 V *vs.* $Li^+/Li$ and a slope with an average potential of 1.75 V *vs.* $Li^+/Li$. Excellent cycling and high rate performance are observed when r-LVP/C is used as a cathode. We report for the first time that two more Li can be inserted into the r-LVP structure, which is different from its sodium counterpart where only one Na could be inserted. We investigated the lithium storage mechanism of r-LVP/C by *in situ* XRD and revealed a typical solid-solution reaction. Symmetrical batteries were also assembled and presented a high capacity of 120 mA h $g^{-1}$ with an operating voltage of ~2.0 V.

## 2. Experimental section

The carbon-coated rhombohedral $Na_3V_2(PO_4)_3$ compound (r-NVP/C) was synthesized by mixing a stoichiometric amount of $NaH_2PO_4$ (99.9%, Alfa Aesar), $V_2O_3$ (99.9%, Alfa Aesar) and glucose as carbon source. The mass ratio of $V_2O_3$ and glucose is 3.5 : 1, which means the expected carbon content in the product is about 5%. The precursors were ball-milled and then calcined at 800 °C for 12 hours. The obtained r-NVP/C sample (1 g) was added to 1 M $LiPF_6$ in EC : DEC electrolyte (10 mL) and stirred overnight. The samples were centrifuged and washed with DI water several times. The process was repeated twice to maximize the degree of ion exchange. The final sample was dried at 60 °C for 8 hours.

r-LVP/C was structurally characterized by XRD using a Bruker D8 Advance diffractometer using Cu Kα radiation (1.5405 Å). The morphology characterization was investigated using a scanning electron microscope (SEM, LEO Gemini 1525) and a transmission electron microscope (TEM, JEOL 2100F) operated at 200 keV. The carbon content was determined by thermogravimetric analysis (TGA).

A slurry containing 70 wt% r-LVP/C composite, 20 wt% carbon conductive additive and 10 wt% polyvinylidene fluoride (PVdF) was cast on an Al foil and dried in vacuum at 100 °C for 10 hours. The coin cells were assembled with Li metal as counter electrode with 1 M $LiPF_6$ EC : DEC (1 : 1) as electrolyte in an argon-filled glove box. The mass loading of the active materials was 2 mg $cm^{-2}$. Electrochemical measurements were performed using a LAND BT2000 battery cycler. For *in situ* XRD measurements, an r-LVP/C electrode was used as a working electrode obtained by immersing an r-NVP/C electrode in 1 M $LiPF_6$ in an EC : DEC electrolyte. Polytetrafluoroethylene (PTFE) was used as the binder, and aluminium mesh was used as the current collector. Symmetrical cells were assembled by using r-LVP/C as active materials for both the cathode and the anode, where the mass ratio between cathode and anode is about 1 : 1.12. Discharge/charge tests were measured in the voltage range 3.2–0 V.

## 3. Results and discussion

The r-NVP/C sample was synthesized in a one-step solid-state reaction as reported in a previous study.[38] The r-LVP/C sample was prepared using a facile ion-exchange method (see Experimental section). Inductively coupled plasma (ICP) was performed to identify the composition of the ion-exchange product. The result shows that the ratio of Li : Na : V is 2.832 : 0.168 : 1.991, corresponding to a composition of $Li_{2.83}Na_{0.17}V_2(PO_4)_3$, indicating nearly complete ion exchange. Fig. 1a shows that the XRD peak positions and the relative intensity of the r-LVP/C sample are different from those of the r-NVP/C sample. The peaks of the r-LVP/C sample shift from low angles to high angles, and the strongest diffraction peak (113) shifts from 27.7° to 28.4°. Rietveld-refined XRD was conducted to further investigate the detailed structure of r-LVP; the results are shown in Fig. 1b, and the crystal parameters are summarized in Table S1.† The obtained parameters are reliable: $R_p$ = 14.8; $R_{wp}$ = 13.4; and $R_{exp}$ = 9.1. All of the diffraction peaks of the r-LVP/C sample are indexed to a rhombohedral system with a space group of $R\bar{3}$ (Fig. 1a), which is different from the space group of $R\bar{3}$ C for r-NVP. The lattice constants of r-LVP ($a = b$ = 8.329 Å, $c$ = 22.518 Å) are determined from Rietveld-refined

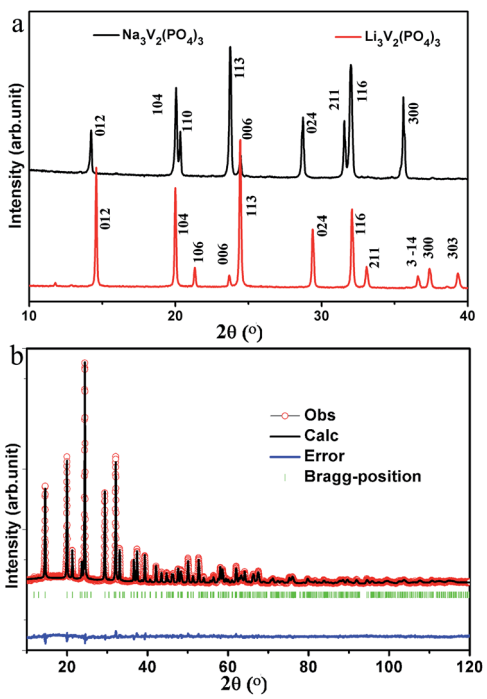


Fig. 1 (a) XRD patterns of the r-NVP/C and r-LVP/C samples. (b) Rietveld-refined XRD results of the r-LVP/C sample, in which observed data are indicated by the red symbols and the calculated profile is represented by the black dotted line overlaying the red symbols. The residual discrepancy is shown in blue.

XRD. After the ion exchange, the skeleton structure still remains and shares the corners of $VO_6$ octahedra and $PO_4$ tetrahedra. The *c* parameter of the unit cell slightly increases from 21.815 Å in r-NVP to 22.518 Å in r-LVP, which could be attributed to the strong electrostatic repulsion between $VO_6$ octahedra along the *c* axis after the $Na^+$ ion is replaced by the $Li^+$ ion.

The schematic diagrams for the structure of r-LVP and r-NVP are shown in Fig. 2. In the structure of r-LVP, the vanadium sites split into two distinct sites in the space group of $R\bar{3}$, resulting in two extra peaks at 11.7° and 12.9° in the powder diffraction pattern compared with the r-NVP structure (magnified XRD pattern in Fig. S1†). Phosphorus is still located at a single crystallographic site, forming $PO_4$ tetrahedra with oxygen. Li atoms fully occupy new crystallographic sites (18f), which are different from the original Na sites (6b and 18e), possibly due to the smaller ionic radii and (or) positional difference between $Na^+$ and $Li^+$.[39] The framework $[V_2(PO_4)_3]_\infty$ is parallel to the (a and b) plane, whereas $Li^+$ ion layers are perpendicular to the *c* axis. The remaining $Na^+$ ions in the ion-exchanged r-LVP/C sample occupy 3a and 3b sites, which are equivalent to the 6b site in the r-NVP structure.

SEM results (shown in Fig. S3†) show the similar morphology of the r-NVP/C and r-LVP/C samples. High-resolution transmission electron microscopy (HRTEM) was further carried out to investigate the r-NVP/C and r-LVP/C samples. After the ion exchange, carbon is still uniformly coated on the surface (Fig. 3a and b); this result indicates that the ion-exchange method is successful. However, we could not observe the peak of carbon in the XRD pattern, indicating that the carbon coating layer is amorphous, which is in good agreement with the TEM result. Fig. 3c and d provide the lattice structures of the r-NVP/C and r-LVP/C samples. In the r-NVP/C sample, the lattice spacing of $d =$ 0.38 nm corresponds to the (113) plane, which reflects the highest diffraction peak among the XRD peaks. The lattice spacing in the r-LVP/C sample is $d = 0.36$ nm. The radius of $Li^+$ is considerably smaller than that of $Na^+$. When the $Li^+$ replaces the $Na^+$, the unit cell volume will shrink, leading to a reduced lattice spacing. The volume change from r-NVP to r-LVP is *ca.* 6%, which further proves the success of ion exchange. These results are consistent with the XRD data in that all diffraction peaks shift to higher angles. The carbon content of the two samples before and after ion exchange was determined by TGA (Fig. S2†), which shows that the carbon content increases from 5.4% (carbon in r-NVP/C sample) to 6.6% (carbon in the r-LVP/C sample).

Fig. 4a shows the cyclic voltammetry (CV) analysis of the r-LVP/C electrode at a scan rate of 0.05 mV $s^{-1}$ in the voltage range 3.0 V to 4.5 V *vs.* $Li^+$/Li. A pair of redox peaks is clearly observed at 3.64 and 3.89 V *vs.* $Li^+$/Li, higher than those of the

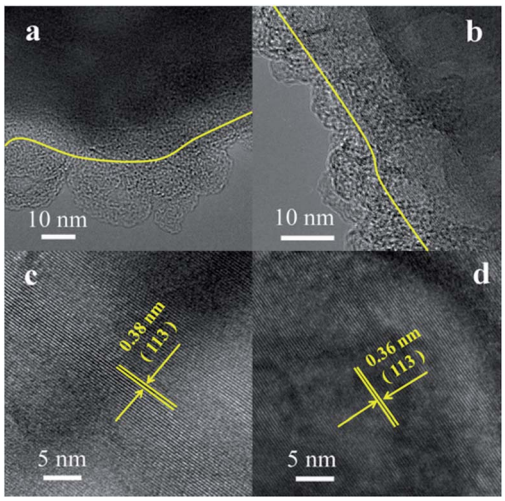


Fig. 3 TEM images of the (a) r-NVP/C and (b) r-LVP/C samples. HR-TEM images of the (c) r-NVP/C and (d) r-LVP/C samples showing lattice information.

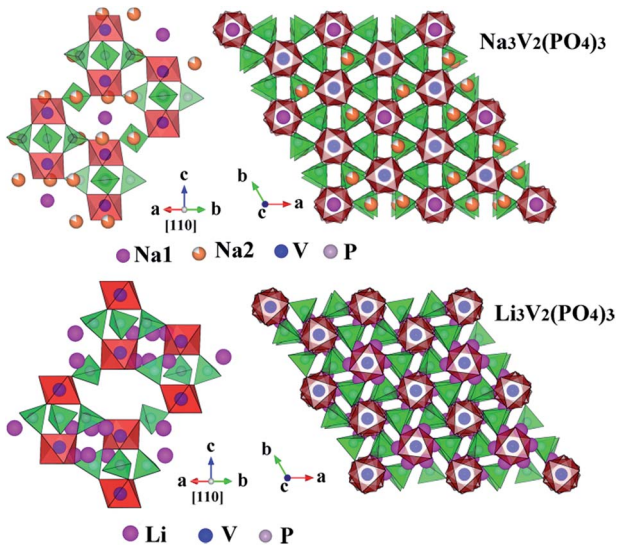


Fig. 2 Schematic diagram of structures of $Na_3V_2(PO_4)_3$ (upper) and $Li_3V_2(PO_4)_3$ (lower).

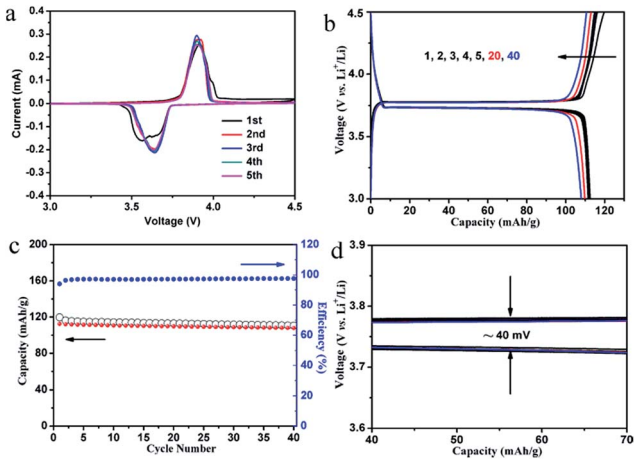


Fig. 4 (a) CV curves of the r-LVP/C electrode in a voltage range of 3.0 V to 4.5 V at a scan rate of 0.05 mV $s^{-1}$; (b) selected charge/discharge curves of the r-LVP/C electrode at a rate of 0.1 C; (c) cycling performance of the r-LVP/C electrode at 0.1 C; and (d) the magnified flat region of the charge/discharge curves.

r-NVP/C–Na cell by approximately 0.3 V because $Li^+/Li$ exhibits a lower redox voltage than that of $Na^+/Na$. Since no other peak could be observed from the CV curves, the pair of redox peaks should correspond to the $V^{3+}/V^{4+}$ redox couple. In the first cycle, the redox peaks are slightly broader than those in the following cycles, which is probably due to the presence of residual $Na^+$ ions that have not been ion-exchanged completely. The subsequent CV curves almost overlap, indicating an excellent cycling performance. Fig. 4b shows the charge/discharge curves of the r-LVP/C electrode during the first five cycles, 20$^{th}$ cycle and 40$^{th}$ cycle at a rate of 0.1 C. There is a very flat plateau at 3.75 V *vs.* $Li^+/Li$, which is consistent with the CV result. The r-LVP/C sample delivers an initial charge capacity of 120 mA h $g^{-1}$ and a high reversible discharge capacity of 113 mA h $g^{-1}$. Taking the presence of 6.6% carbon in the r-LVP/C sample into account, the observed capacity (121 mA h $g^{-1}$) is very close to the theoretical value (131 mA h $g^{-1}$) for the two Li insertion. The reason that only two-thirds of the Li ions could be extracted from the structure is because once two-thirds of Li ions were extracted from the tetrahedral sites, the remaining one-third of Li ions will diffuse to 3a or 3b sites and could not be further extracted.[18] Fig. 4c shows the cycling performance. After 40 cycles, reversible capacity could be maintained at 108 mA h $g^{-1}$, which is 96% of the original reversible capacity. The initial coulombic efficiency is 94.2% and increases to 99% in later cycles. The magnified flat regions of the charge/discharge curves are shown in Fig. 4d. The voltage hysteresis of only ~40 mV is very small and does not increase during the 40 cycles, indicating excellent electronic and ionic conductivity and great stability. Overall the r-LVP/C sample shows excellent electrochemical performance.

We investigated the rate capability of the r-LVP/C sample and compared it with that of the r-NVP/C sample. Fig. 5a shows that the r-LVP/C electrode generally exhibits a higher capacity than that of its sodium counterpart, particularly at high rates (2 C and 5 C). r-LVP has a larger theoretical capacity (131 mA h $g^{-1}$) than that of r-NVP (117 mA h $g^{-1}$). Therefore, the difference at low rates in capacity is small because both samples can approach their theoretical capacity. At higher rates, r-LVP/C shows a reversible capacity of 97.7 and 76 mA h $g^{-1}$ at 2 C and 5 C, respectively. In comparison, r-NVP/C shows a reversible capacity of only 57 and 8 mA h $g^{-1}$. This difference in the rate performance is mainly due to the smaller ionic radius of $Li^+$ than that of $Na^+$.

The charge/discharge voltage profiles at different C-rates are shown in Fig. 5b. The reversible capacities are 111.4, 110.6, 108.2, 103.8, 97.7 and 76 mA h $g^{-1}$ at 0.1 C, 0.2 C, 0.5 C, 1 C, 2 C and 5 C, respectively. Its capacity remains almost unchanged at low rates. Even at 2 C and 5 C, the capacity remains at approximately 87.7% and 68.2% of the original capacity (0.1 C), respectively. Furthermore, voltage hysteresis slightly increases with the C-rate increasing. Even at 2 C, its overvoltage is only ~240 mV. The excellent C-rate performance of the r-LVP/C sample could be attributed to the uniform carbon coating and the inherently high ionic conductivity of the NASICON structure. The long cycling performance is shown in Fig. 5c. After 300 cycles at 1 C, capacity is still higher than 90 mA h $g^{-1}$ and it shows a high coulombic efficiency of ~99%. A good long cycling performance is attributed to the uniform carbon coating and minimum volume change during charge/discharge. The carbon coating layer can prevent r-LVP from directly interacting with electrolytes, thereby inhibiting any side reaction.

*Ex situ* XRD is conducted to understand the lithium storage mechanism of r-LVP. Fig. 6 shows the XRD patterns of the r-

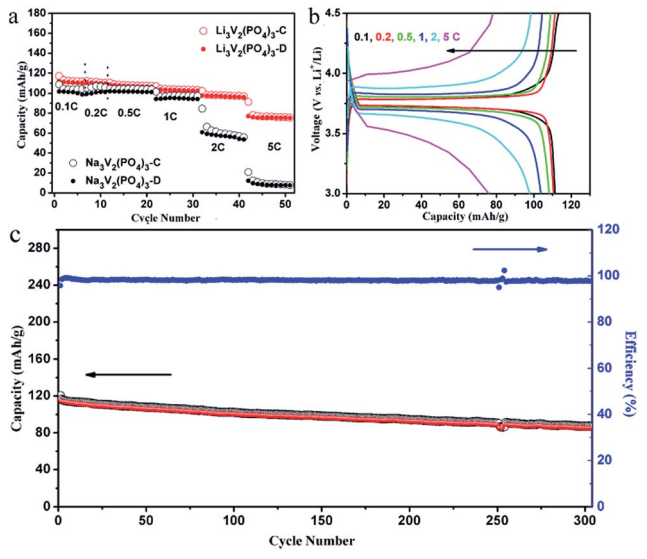


Fig. 5 (a) Rate performance of r-LVP/C and r-NVP/C; (b) typical charge/discharge curves of the r-LVP/C electrode at different C-rates; 1 C refers to the two Li extraction from r-LVP per formula unit in 1 hour; (c) 300 cycles of r-LVP/C at 1 C with 77% capacity retention.

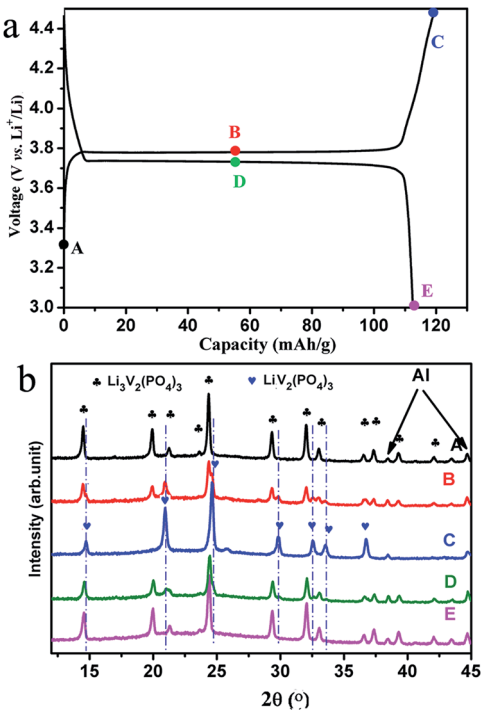


Fig. 6 *Ex situ* XRD patterns (b) of the r-LVP/C electrode at various states of charge indicated in the voltage profile (a).

LVP/C electrode with various states of charge (Fig. 6a): pristine (A), half-charged (B), fully charged (C), half-discharged (D) and fully discharged (E). Peaks of the aluminum substrate are observed near 38.5° and 44.7°. New diffraction peaks, such as 21°, 24.7°, 29.9°, 32.6° and 33.7° (marked by blue ♥), are observed when the electrode is in a half-charged state. The new diffraction peaks shift from low angles to high angles (C), corresponding to a decrease in the crystalline interplanar spacing that resulted from the Li extraction. Considering the electrochemical result, we conclude that the new diffraction peaks belong to rhombohedral $LiV_2(PO_4)_3$. Two phases also coexist in the 50% discharged state (D). All diffraction peaks revert to those of the r-LVP structure when the electrode is fully discharged (E). *Ex situ* XRD results indicate that the mechanism of lithium storage in r-LVP is a typical two-phase reaction, which is similar to that of its sodium counterpart. However, the volume change of approximately 6.11% is considered small,[25] even smaller than that of $LiFePO_4$ (6.81%).[9] The completely reversible structural evolution in the charge/discharge process is closely related to the stable cycling of the r-LVP/C sample.

As is known, r-NVP/C (ref. 38) and m-LVP (ref. 40) can also be used as anodes for sodium-ion batteries. Only one Na can insert into the r-NVP structure[38] and two Li can insert into the m-LVP structure.[40] Here, we investigated the Li insertion capability of r-LVP/C. The discharge/charge curves in the voltage range 3.0–1.0 V *vs.* $Li^+/Li$ are shown in Fig. 7a. The initial discharge/charge capacity is 136/117 mA h $g^{-1}$ at a rate of 0.1 C, which corresponds to a two Li insertion into the r-LVP structure. Its subsequent discharge/charge curves almost overlap, indicating good cycling performance. The long cycling performance at a rate of 1 C is shown in Fig. 7b, which shows an initial reversible capacity of 98.3 mA h $g^{-1}$. The subsequent coulombic efficiency is close to 100% and the capacity retention is 76% over 500 cycles.

Furthermore, we find that discharge/charge curves show a sloping profile with average voltage of 1.75 V *vs.* $Li^+/Li$, which is very different from the discharge/charge curves of the r-NVP/Na cell (Fig. S4†), indicating a different storage mechanism. Five Li can be accommodated in the r-LVP structure while only four Na can be accommodated in the r-NVP structure. This can be ascribed to the difference in the space groups of r-LVP and r-NVP and the ionic radii of lithium and sodium. Two additionally inserted Li atoms will occupy 3a (0.5 Li), 3b (0.5 Li) and 6c (1 Li) as in the schematic diagram shown in Fig. 8a. Fig. 8b shows the *in situ* XRD result of r-LVP/C during the discharge and charge processes. We observed a continuous shift of diffraction peaks to lower angles when Li was inserted during the discharge process, and peaks shift to higher angles when Li was extracted during the charge process. This result indicates a typical solid-solution reaction.

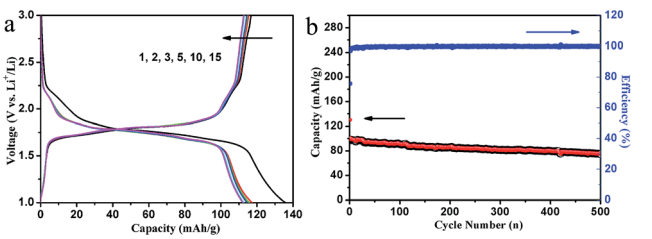


Fig. 7 (a) Selected discharge/charge curves of the r-LVP/C electrode at a rate of 0.1 C in the voltage range of 3.0–1.0 V *vs.* $Li^+/Li$; (b) 500 cycles of r-LVP/C at 1 C with 76% capacity retention.

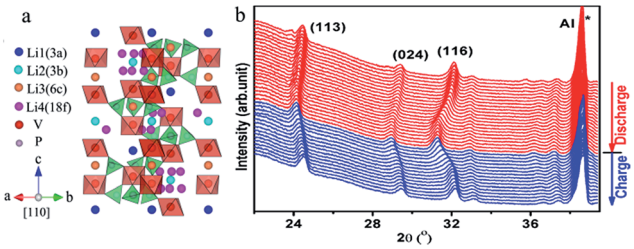


Fig. 8 (a) Possible structure of r-LVP after two more Li insertion at [110] orientation; (b) *in situ* XRD patterns of the r-LVP/C–Li battery cycled at voltages of 3.0 and 1.0 V *vs.* $Li^+/Li$ at a rate of 0.1 C.

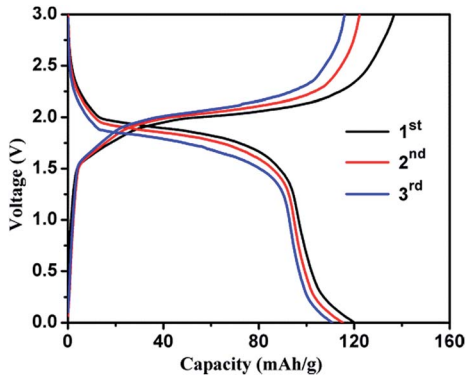


Fig. 9 The charge/discharge profiles of the symmetrical full cell in $LiPF_6$/EC + DEC electrolyte at a current rate of 0.1 C in a voltage range of 3.2–0 V. (The capacity is calculated based on the mass of the cathode. The capacity ratio of cathode:anode is 1 : 1.12.).

Since r-LVP/C can be oxidized (two Li extraction) at 3.75 V *vs.* $Li^+/Li$ and be reduced (two Li insertion) at an average potential of 1.75 V *vs.* $Li^+/Li$, respectively, this material could be assembled into a symmetrical full cell, *i.e.* r-LVP/C was used as both the cathode and the anode. Fig. 9 shows that the full cell delivers an average operating voltage of about 2.0 V, which is in good agreement with the theoretical output voltage. The reversible capacity can reach 120 mA h $g^{-1}$ (based on the weight of cathode material). The energy density of the symmetrical full cell based on the total mass of cathode and anode (in a 1 : 1.12 ratio) is 113 W h $kg^{-1}$, which can be potentially used for large-scale energy storage. Further optimization of the symmetrical full cell is in progress.

## 4. Conclusions

In summary, carbon-coated r-LVP samples were synthesized by the ion-exchange method. After the ion exchange, the structure evolved from the $R\bar{3}$ C group to the $R\bar{3}$ group. All Li atoms occupy the same sites (18f) in the r-LVP structure. The r-LVP/C

sample shows a flat plateau at 3.75 V *vs.* $Li^+$/Li with a very small overpotential (~40 mV) and a slope with the average voltage at 1.75 V *vs.* $Li^+$/Li. When used as a cathode, r-LVP/C exhibits excellent rate and long cycling performance. At 2 C and 5 C, the reversible capacity can reach 97.7 and 76 mA h $g^{-1}$, respectively. The capacity remains at 90 mA h $g^{-1}$ after 300 cycles at a rate of 1 C. *Ex situ* XRD results indicate that the lithium storage mechanism is a typical two-phase reaction with a small volume change of 6.11%. The reversible structural change during the charge/discharge process contributes to the excellent electrochemical performance of the r-LVP/C sample. Further study indicates that the r-LVP/C sample can also be used as an anode for LIBs, which delivers a reversible capacity of 117 mA h $g^{-1}$ (two Li insertion). Its capacity retention rate is 76% over 500 cycles at 1 C. These excellent properties make r-LVP a promising candidate for both cathode and anode for LIBs. A symmetrical full cell exhibits a reversible capacity of 120 mA h $g^{-1}$ with an operating voltage of ~2.0 V.

## Acknowledgements

Y. Y. acknowledges the support from National Science Foundation (CMMI-1400261), Robert A. Welch Professorship at TcSUH (E-0001). Y. S. Hu acknowledges the support from NSFC (51222210 and 11234013, China). W. Han acknowledges the support from NSFC (11205249, China).

## Notes and references

1 M. Armand and J.-M. Tarascon, *Nature*, 2008, **451**, 652–657.
2 H. Li, Z. Wang, L. Chen and X. Huang, *Adv. Mater.*, 2009, **21**, 4593–4607.
3 B. Kang and G. Ceder, *Nature*, 2009, **458**, 190–193.
4 M. S. Whittingham, *MRS Bull.*, 2008, **33**, 411–419.
5 R. Van Noorden, *Nature*, 2014, **507**, 26–28.
6 M. S. Whittingham and T. Zawodzinski, *Chem. Rev.*, 2004, **104**, 4243–4244.
7 D. J. Klionsky, F. C. Abdalla, H. Abeliovich, R. T. Abraham, A. Acevedo-Arozena, K. Adeli, L. Agholme, M. Agnello, P. Agostinis and J. A. Aguirre-Ghiso, *Autophagy*, 2012, **8**, 445–544.
8 Y. G. Guo, J. S. Hu and L. J. Wan, *Adv. Mater.*, 2008, **20**, 2878–2887.
9 A. K. Padhi, K. Nanjundaswamy and J. B. Goodenough, *J. Electrochem. Soc.*, 1997, **144**, 1188–1194.
10 Y. Wang, Y. Wang, E. Hosono, K. Wang and H. Zhou, *Angew. Chem.*, 2008, **120**, 7571–7575.
11 A. Yamada, S.-C. Chung and K. Hinokuma, *J. Electrochem. Soc.*, 2001, **148**, A224–A229.
12 D. Choi, D. Wang, I.-T. Bae, J. Xiao, Z. Nie, W. Wang, V. V. Viswanathan, Y. J. Lee, J.-G. Zhang and G. L. Graff, *Nano Lett.*, 2010, **10**, 2799–2805.
13 C. Delacourt, L. Laffont, R. Bouchet, C. Wurm, J.-B. Leriche, M. Morcrette, J.-M. Tarascon and C. Masquelier, *J. Electrochem. Soc.*, 2005, **152**, A913–A921.
14 V. Aravindan, J. Gnanaraj, Y.-S. Lee and S. Madhavi, *J. Mater. Chem. A*, 2013, **1**, 3518–3539.
15 Q. Wei, Q. An, D. Chen, L. Mai, S. Chen, Y. Zhao, K. M. Hercule, L. Xu, A. Minhas-Khan and Q. Zhang, *Nano Lett.*, 2014, **14**, 1042–1048.
16 C. Delmas, A. Nadiri and J. L. Soubeyroux, *Solid State Ionics*, 1988, **28**, 419–423.
17 C. Masquelier, A. Padhi, K. Nanjundaswamy and J. Goodenough, *J. Solid State Chem.*, 1998, **135**, 228–234.
18 S.-C. Yin, H. Grondey, P. Strobel, M. Anne and L. Nazar, *J. Am. Chem. Soc.*, 2003, **125**, 10402–10411.
19 H. Huang, S. C. Yin, T. Kerr, N. Taylor and L. F. Nazar, *Adv. Mater.*, 2002, **14**, 1525–1528.
20 G. Ceder, A. Jain, G. Hautier, J. C. Kim, B. Kang and R. Daniel, Google Patents, 2013, US8399130 B2.
21 A. Jain, G. Hautier, C. Moore, B. Kang, J. Lee, H. Chen, N. Twu and G. Ceder, *J. Electrochem. Soc.*, 2012, **159**, A622–A633.
22 P. Barpanda, T. Ye, S.-C. Chung, Y. Yamada, S.-i. Nishimura and A. Yamada, *J. Mater. Chem.*, 2012, **22**, 13455–13459.
23 M. Tamaru, P. Barpanda, Y. Yamada, S.-i. Nishimura and A. Yamada, *J. Mater. Chem.*, 2012, **22**, 24526–24529.
24 H.-P. Hong, *Mater. Res. Bull.*, 1978, **13**, 117–124.
25 V. Thangadurai and W. Weppner, *Ionics*, 2002, **8**, 281–292.
26 J. Shi, G. Yin, L. Jing, J. Guan, M. Wu, Y. Zhou, H. Lou and Z. Wang, *Int. J. Mod. Phys. B*, 2014, **28**, 1450176.
27 D. Han, S.-J. Lim, Y.-I. Kim, S. H. Kang, Y. C. Lee and Y.-M. Kang, *Chem. Mater.*, 2014, **26**, 3644–3650.
28 J. Gaubicher, C. Wurm, G. Goward, C. Masquelier and L. Nazar, *Chem. Mater.*, 2000, **12**, 3240–3242.
29 Y. Lu, L. Wang, J. Song, D. Zhang, M. Xu and J. B. Goodenough, *J. Mater. Chem. A*, 2013, **1**, 68–72.
30 M. Ren, Z. Zhou, X. Gao, W. Peng and J. Wei, *J. Phys. Chem. C*, 2008, **112**, 5689–5693.
31 Y. Luo, X. Xu, Y. Zhang, Y. Pi, Y. Zhao, X. Tian, Q. An, Q. Wei and L. Mai, *Adv. Energy Mater.*, 2014, DOI: 10.1002/aenm.201400107.
32 J. Xu, S.-L. Chou, C. Zhou, Q.-F. Gu, H.-K. Liu and S.-X. Dou, *J. Power Sources*, 2014, **246**, 124–131.
33 J. Wang and X. Sun, *Energy Environ. Sci.*, 2012, **5**, 5163–5185.
34 G.-N. Zhu, H.-J. Liu, J.-H. Zhuang, C.-X. Wang, Y.-G. Wang and Y.-Y. Xia, *Energy Environ. Sci.*, 2011, **4**, 4016–4022.
35 Z. Jian, L. Zhao, R. Wang, Y.-S. Hu, H. Li, W. Chen and L. Chen, *RSC Adv.*, 2012, **2**, 1751–1754.
36 B. L. Cushing and J. B. Goodenough, *J. Solid State Chem.*, 2001, **162**, 176–181.
37 S. Li, Y. Dong, L. Xu, X. Xu, L. He and L. Mai, *Adv. Mater.*, 2014, **26**, 3358.
38 Z. Jian, L. Zhao, H. Pan, Y.-S. Hu, H. Li, W. Chen and L. Chen, *Electrochem. Commun.*, 2012, **14**, 86–89.
39 Z. Jian, C. Yuan, W. Han, X. Lu, L. Gu, X. Xi, Y. S. Hu, H. Li, W. Chen and D. Chen, *Adv. Funct. Mater.*, 2014, **24**, 4265–4272.
40 A. S. Hameed, M. V. Reddy, B. V. R. Chowdari and J. J. Vittala, *Electrochim. Acta*, 2014, **128**, 184–191.

 